

11. J. A. Dumesic *et al.*, in *New Frontiers in Catalysis, Proceedings of the 10th International Congress on Catalysis, Budapest, Hungary*, L. Guzzi *et al.*, Eds. (Akadémiai Kiadó, Budapest, 1993), p. 1325.
12. See the comments by G. C. Bond and the other discussions following (11).
13. N.-Y. Topsøe and H. Topsøe, *Catal. Today* **9**, 77 (1991).
14. G. Busca, *Langmuir* **2**, 577 (1986).
15. G. T. Went, S. T. Oyama, A. T. Bell, *J. Phys. Chem.* **94**, 4240 (1990).
16. J. R. Rostrup-Nielsen, in *Elementary Reaction Steps in Heterogeneous Catalysis*, R. W. Joyner and R. A. van Santen, Eds. (Kluwer Academic, Dordrecht, Netherlands, 1993), pp. 441–460.
17. M. Boudart, paper presented at the American Chemical Society 1994 spring San Diego meeting, Symposium on Catalytic Reaction Engineering for

- Environmentally Benign Processing.
18. J. A. Dumesic *et al.*, in *The Microkinetics of Heterogeneous Catalysis* (American Chemical Society, Washington, DC, 1993).
 19. I acknowledge helpful discussions with H. Topsøe, J. A. Dumesic, and E. G. Derouane.

23 May 1994; accepted 11 July 1994

The Spatial Structure in Liquid Water

Peter G. Kusalik* and Igor M. Svishchev

Liquid state structure has traditionally been characterized with the radial distribution functions between atoms. Although these functions are routinely available from x-ray diffraction and neutron scattering experiments or from computer simulations, they cannot be interpreted unambiguously to provide the spatial order in a molecular liquid. A direct approach to determining the spatial structure in the liquid state is demonstrated here. Three-dimensional maps representing the local atomic densities are presented for several water models. These spatial maps provide a picture of the short-range order in liquid water which reveals specific details of its local structure that are important in the understanding of its properties.

The unusual physical properties of liquid water, in which its structure plays a key role, have long challenged researchers and have resulted in numerous theoretical and phenomenological models (1–4). The tendency for tetrahedral arrangements in liquid water structure is well established. However, the nature and role of the additional, nontetrahedral coordination that is believed to exist in water have been the subject of extensive debate and speculation (1, 4–6). Although much of the controversy associated with understanding water structure could be resolved if the details of the full three-dimensional (3D) local molecular packing were available, experimental structural studies of water have been restricted to the orientationally averaged (or spatially folded) radial distribution functions (RDFs) between the oxygen (O) and hydrogen (H) atoms, specifically $g_{OO}(r)$, $g_{OH}(r)$, and $g_{HH}(r)$ (7, 8). These functions, which represent the probability of finding a second particle at a separation r from a first, can provide only limited information on the local structure in a molecular system. Unfortunately, computer simulation methods (9, 10) have also relied almost exclusively on RDFs. In a computer simulation study of SPC/E water (11, 12) we overcame the limitations of RDFs by determining the spatial distribution functions (SDFs), $g_{OO}(r, \Omega)$ and $g_{OH}(r, \Omega)$, for oxygen and hydrogen atoms. While still being a contraction of the full two-molecule distribution function, these SDFs span both the radial, r , and

angular, Ω , coordinates of the interatomic separation vector (13) and hence are sufficient to characterize the local 3D packing of molecules. These spatial maps confirm a tetrahedral network pattern of hydrogen (H)-bonded molecules and, for the SPC/E model of liquid water, establish the existence of separate maxima in the local atomic density at “interstitial” (nontetrahedral) positions.

Here we compare the average local structure, as given by the SDF, within several models for liquid water at 25°C and demonstrate that nontetrahedral coordination arises independently of the choice of interaction potential. Hence, we conclude that this structural feature is a general result characteristic of the real system. Along with SPC/E water, the TIP4P potential (14) as well as the recently developed polarizable

point charge (PPC) water model (15) are considered in this computer simulation study; these models and some of their average properties are summarized in Table 1. All three models successfully reproduce some of the bulk properties of liquid water, as can be seen from Table 1, and their RDFs $g_{OO}(r)$, shown in Fig. 1, are all in good agreement with experimental data (7).

The oxygen-oxygen spatial distribution function for the TIP4P and PPC potentials are compared in Fig. 2, where $g_{OO}(r, \Omega)$ have been visualized as 3D oxygen density maps. These SDFs are rich in detail and correctly portray water as a highly structured liquid. We see that the two model liquids share the same principal structural features: the two distinct caps centered directly over the hydrogens of the central molecule due to its two H-bond-accepting neighbors, the single cupped feature below the central molecule due to its two H-bond-donating neighbors, and the two more distant (predominantly blue) features due to additional nontetrahedral coordination. The blue color of this additional coordination emphasizes that these local maxima in oxygen density (which contain roughly one neighbor) occur at separations corresponding to the first minimum in $g_{OO}(r)$ (see Fig. 1). It is these local maxima, which are lost when the angle-averaged RDF is formed, that lead to the elevated pair-density observed around the first minimum in $g_{OO}(r)$. Earlier studies attempting to identify this “interstitial” maximum from the 1D function $g_{OO}(r)$ had led

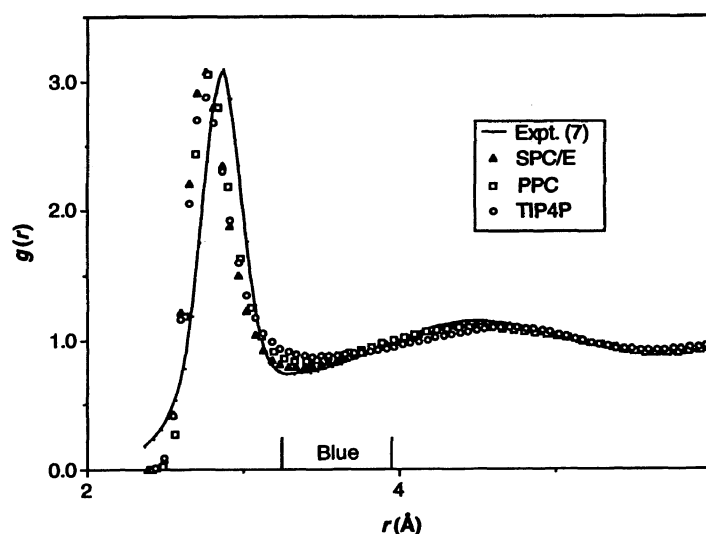


Fig. 1. Comparison of the oxygen-oxygen RDF, $g_{OO}(r)$, for liquid water and the TIP4P, SPC/E, and PPC models for water at 25°C. Also indicated is the range of separations colored blue in Figs. 2 and 4.

Department of Chemistry, Dalhousie University, Halifax, Nova Scotia, B3H 4J3, Canada.

*To whom correspondence should be addressed.

Table 1. Electrostatic, geometric, and Lennard-Jones parameters and values for the average total energies, dielectric constants, and self-diffusion coefficients at 25°C for the three water models under investigation. q_H is the charge on the hydrogen site, μ is the molecular dipole moment expressed in debyes, R_{OH} is the oxygen-hydrogen distance, $\angle HOH$ is the bond angle, and l is the position of the negatively charged site from the oxygen nucleus (the origin) as measured along the symmetry axis. ϵ_{LJ} and σ are the well depth and diameter, respectively, of the Lennard-Jones potential acting between the molecules. $\langle U \rangle$ is the average total configurational energy, ϵ is the static dielectric

Model	q_H	μ (D)	R_{OH} (Å)	$\angle HOH$	l (Å)	ϵ_{LJ} (kJ/mol)	σ (Å)	$\langle U \rangle$ (kJ/mol)	ϵ	D (cm ² /s)
SPC/E*	0.4238	2.35	1.0	109.47°	0	0.65	3.166	-41.5	71	2.2×10^{-5}
TIP4P†	0.52	2.18	0.9572	104.52°	0.15	0.648	3.1536	-41.8	53‡	2.9×10^{-5}
PPC§	0.517¶	2.52¶	0.943	106°	0.06¶	0.6	3.234	-43.2	77	2.6×10^{-5}
Expt.								-41.5	78.3	2.3×10^{-5}

*A 0.5-ns run with $n = 256$ (19).

†A 0.15-ns run with $n = 108$.

‡Measured at 20°C (20).

§A 0.5-ns run with $n = 256$.

¶Average values.

constant, and D is the self-diffusion coefficient. Details regarding our molecular dynamics simulation methodology can be found in (17) and (19). Our simulations were performed at the experimental density for water at 25°C. The PPC model we used retains most of the simplicity of popular three-site water models while incorporating the electrostatic response of the water molecule to a homogeneous applied electric field (representing the local field in the condensed state) as determined from ab initio calculations. For present purposes it is sufficient to note that the PPC model utilizes quantum chemically determined values for its three site charges and geometric parameters (19).

Fig. 2. The spatial distribution function $g_{OO}(r, \Omega)$ for (A) TIP4P and (B) PPC water at 25°C. The isosurfaces corresponding to $g_{OO}(r, \Omega) = 1.4$ are shown; the enclosed regions have average oxygen densities at least 40% greater than that of the bulk. The central molecule has been included to define the local frame. The surfaces are colored according to their distance from the central molecule (see Fig. 1). Ordered by increasing separation, orange to yellow corresponds to $r < 3.2$ Å, green to blue and back to green corresponds to $3.2 \text{ Å} < r < 4.0$ Å, and yellow to red represents r between 4.0 and 5.0 Å.

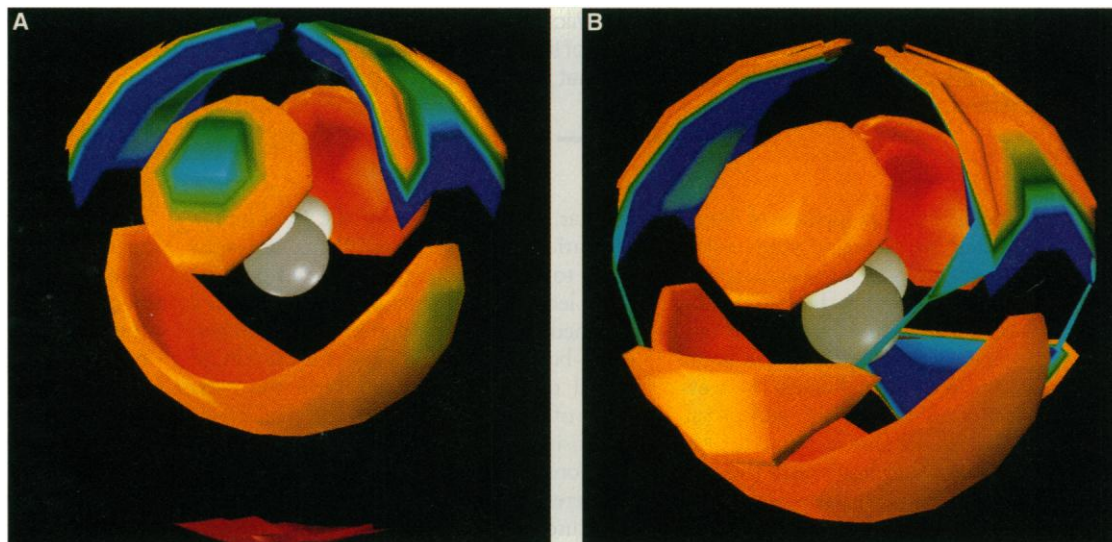


Fig. 3. The spatial distribution functions $g_{OO}(r, \Omega)$ and $g_{OH}(r, \Omega)$ for SPC/E water at 25°C. The blue isosurfaces correspond to $g_{OH}(r, \Omega) = 1.4$; the regions enclosed by these surfaces have average hydrogen densities at least 40% greater than that of the bulk. The superimposed red isosurfaces represent $g_{OO}(r, \Omega) = 6.0$. The central molecule has been included to define the local frame, and only one hemisphere of the full distribution is shown. The greenish-blue feature in the plane perpendicular to the molecular plane represents hydrogen density due to molecules in interstitial positions, as discussed in the text.



to numerous speculations on the structure in liquid water (such as “mixture” versus “continuum” models) (1). There is no evidence in Fig. 2 to support the hypothesis of bifurcated H-bonds in water struc-

ture (4), at least for the systems studied.

Some subtle but important differences in the local spatial structures of these model water systems (inaccessible through the RDF) can also be identified from figures

similar to Fig. 2. At the threshold used in Fig. 2, the equivalent map for SPC/E water lies essentially “between” the TIP4P and PPC results. On reduction of the threshold we find that the secondary (second and third neighbor) structure “below” the oxygen site of the central molecule is more pronounced in TIP4P than in either PPC or SPC/E water (this is intimated by the red feature near the bottom of Fig. 2A), whereas the secondary structure “above” the hydrogen sites is the least developed in the TIP4P system. In Fig. 2 we also observe that the PPC spatial map processes two extra nontetrahedral features near the plane of the central molecule not evident in the TIP4P function at this threshold.

One of the most interesting features of the local structure that appears in these spatial maps on reduction of the threshold is a “bridge” in the oxygen density. This bridge forms between the feature representing the H-bond-donating neighbors (below the central molecule) and the nontetrahedral (interstitial) coordination. This structural pattern is a manifestation of the cou-

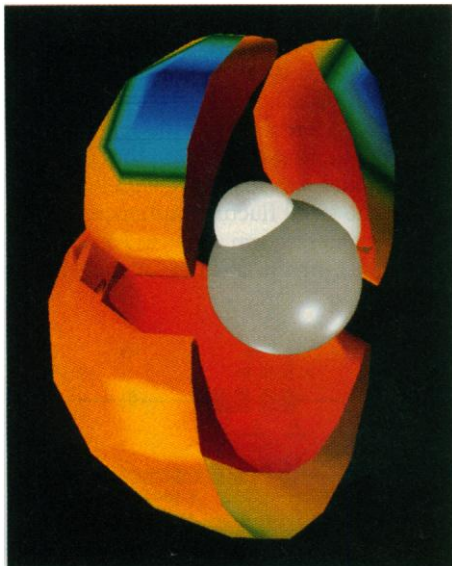


Fig. 4. The spatially resolved average pair interaction energy $\langle u_i(r, \Omega) \rangle$ for SPC/E water at 25°C. The isosurfaces represent $\langle u_i(r, \Omega) \rangle = -10$ kJ/mol, and hence, any molecules found within the regions enclosed by these surfaces interact with the central molecule on average with an energy less than -10 kJ/mol. Only one hemisphere of the full distribution is shown where the central molecule has been included to define the local frame. The surfaces have been colored according to their separation as in Fig. 2.

pling of certain rotational and translational motions of the central molecule (12) (this “rocking” motion of water molecules also accounts for the single feature due to the two H-bond-donating neighbors). This bridge between the H-bond-donating neighbors and the nontetrahedral coordination becomes evident in the oxygen density map at a higher threshold [$g_{OO}(r, \Omega) \approx 1.25$] for TIP4P than for either PPC or SPC/E water [$g_{OO}(r, \Omega) \approx 1.15$], indicating stronger couplings in the former liquid.

Further insights into the local structure in these liquids are provided in Fig. 3, which shows an overlay of the hydrogen and oxygen density maps for SPC/E water. The hydrogens of the H-bond-donating neighbors are clearly resolved into two cupped features “sandwiching” the oxygen density below the central molecule, whereas the two hydrogens of each of the H-bond-accepting neighbors appear as single featureless caps somewhat beyond their respective oxygen features above the central molecule. Figure 3 exhibits one additional hydrogen feature due to the neighbors in nontetrahedral coordination. This local maximum in the hydrogen density appears at separations of 4.0 to 4.4 Å, corresponding to the rather shallow second minimum in $g_{OH}(r)$. Behavior similar to that observed in Fig. 3 can be found for the TIP4P and PPC systems.

To demonstrate further the utility of spatial maps (as opposed to simple 1D radial analysis) we have also spatially resolved the average pair interaction energy for SPC/E water. This function is presented in Fig. 4 where isosurfaces corresponding to -10 kJ/mol, an accepted limit for H-bond energies in water (14), are shown. Thus, from an energetic point of view, molecules found within the boundaries of the features in Fig. 4 will on average be “H-bonded” to the central molecule. Comparison of the features due to “H-bonded” neighbors in Figs. 2 (density maps) and 4 (potential map) reveals that, although they are qualitatively similar, a geometric criterion based on the oxygen-oxygen SDF will be more selective. From Fig. 4 we observed that the average pair interaction for nontetrahedral (interstitial) neighbors is greater than -10 kJ/mol, although a significant fraction of the molecules making up this coordination would be labeled as H-bonded from an energetic viewpoint (11).

Soper (16) has argued that the SDF for water can be determined from experimental data. His approach (16, 17) uses a maximum entropy constraint to estimate a full molecular pair distribution function that is consistent with the atom-atom RDFs obtained from neutron scattering (18). Soper’s results [see figure 7 of (16)] strongly support our model calculations.

REFERENCES AND NOTES

1. D. Eisenberg and W. Kauzmann, *The Structure and Properties of Water* (Oxford Univ. Press, Oxford, 1969).
2. M. G. Sceats, M. Stavola, S. A. Rice, *J. Chem. Phys.* **70**, 3927 (1979).
3. O. Ya. Samoilov, *Structure of Aqueous Electrolyte Solutions and the Hydration of Ions* (Consultants Bureau, New York, 1965).
4. P. A. Giguere, *J. Chem. Phys.* **87**, 4835 (1987).
5. C. Corongiu and E. Clementi, *ibid.* **97**, 2030 (1992).
6. G. Ruocco, M. Sampoli, A. Torcini, R. Vallauri, *ibid.* **99**, 8095 (1993).
7. A. K. Soper and M. G. Phillips, *Chem. Phys.* **107**, 47 (1986).
8. A. H. Narten and H. A. Levy, *J. Chem. Phys.* **55**, 2263 (1971).
9. J. P. Hansen and J. R. McDonald, *Theory of Simple Liquids* (Academic Press, London, 1986).
10. M. P. Allen and D. J. Tildesley, *Computer Simulations of Liquids* (Oxford Univ. Press, Oxford, 1987).
11. I. M. Svishchev and P. G. Kusalik, *J. Chem. Phys.* **99**, 3049 (1993).
12. ———, *Chem. Phys. Lett.* **215**, 596 (1993).
13. Averaging over the angular coordinates Ω one can always recover the RDFs.
14. W. L. Jorgensen, J. Chandrasekhar, J. D. Madura, R. W. Impey, M. L. Klein, *J. Chem. Phys.* **79**, 926 (1983).
15. I. M. Svishchev and P. G. Kusalik, unpublished data.
16. A. K. Soper, *J. Chem. Phys.*, in press.
17. ———, C. Andreani, M. Nardone, *Phys. Rev. E* **47**, 2598 (1993).
18. The reliability of this technique is not known, although it can be tested with computer simulation data.
19. I. M. Svishchev and P. G. Kusalik, *J. Phys. Chem.* **98**, 728 (1994).
20. M. Neumann, *ibid.* **85**, 1567 (1986).
21. We are grateful for the financial support of the Natural Sciences and Engineering Research Council of Canada. We also wish to thank A. K. Soper for a preprint copy of his recent manuscript.

20 April 1994; accepted 5 July 1994

Dependence of Enhancer-Mediated Transcription of the Immunoglobulin μ Gene on Nuclear Matrix Attachment Regions

William C. Forrester, Courtney van Genderen, Thomas Jenuwein,* Rudolf Grosschedl†

Transcription of the immunoglobulin μ heavy chain locus is regulated by an intronic enhancer that is flanked on both sides by nuclear matrix attachment regions (MARs). These MARs have now been shown to be essential for transcription of a rearranged μ gene in transgenic B lymphocytes, but they were not required in stably transfected tissue culture cells. Normal rates of transcriptional initiation at a variable region promoter and the formation of an extended deoxyribonuclease I (DNase I)-sensitive chromatin domain were dependent on MARs, although DNase I hypersensitivity at the enhancer was detected in the absence of MARs. Thus, transcriptional activation of the μ gene during normal lymphoid development requires a synergistic collaboration between the enhancer and flanking MARs.

The murine immunoglobulin heavy chain (Ig_H) locus has been studied as a model of tissue-specific gene regulation. Transcriptional control elements reside within the promoters associated with the variable region (V_H) gene segments, the intronic μ enhancer, and the enhancers located at the 3' end of the locus (1). Although these

elements contribute to B cell-specific gene expression in transfection assays, only the intragenic enhancer region has been shown to direct efficiently lymphoid-specific transcription of a rearranged μ gene and heterologous reporter genes in transgenic mice (2). Delineation of this enhancer in transfection assays indicated that a 220-base pair